

The potassium channel subunit $K_{\nu}\beta 1$ serves as a major control point for synaptic facilitation

In Ha Cho^{a,b}, Lauren C. Panzera^{a,b}, Morven Chin^{a,1}, Scott A. Alpizar^{a,b}, Genaro E. Olveda^{a,b}, Robert A. Hill^{a,b}, and Michael B. Hoppa^{a,b,2}

^aDepartment of Biology, Dartmouth College, Hanover, NH 03755; and ^bMolecular and Cellular Biology Graduate Program, Dartmouth College, Hanover, NH 03755

Edited by Lily Yeh Jan, University of California, San Francisco, CA, and approved October 13, 2020 (received for review January 14, 2020)

Analysis of the presynaptic action potential's (AP_{syn}) role in synaptic facilitation in hippocampal pyramidal neurons has been difficult due to size limitations of axons. We overcame these size barriers by combining high-resolution optical recordings of membrane potential, exocytosis, and Ca²⁺ in cultured hippocampal neurons. These recordings revealed a critical and selective role for K_v1 channel inactivation in synaptic facilitation of excitatory hippocampal neurons. Presynaptic K_v1 channel inactivation was mediated by the K_v\beta1 subunit and had a surprisingly rapid onset that was readily apparent even in brief physiological stimulation paradigms including paired-pulse stimulation. Genetic depletion of $K_{\nu}\beta 1$ blocked all broadening of the AP_{syn} during high-frequency stimulation and eliminated synaptic facilitation without altering the initial probability of vesicle release. Thus, using all quantitative optical measurements of presynaptic physiology, we reveal a critical role for presynaptic K_v channels in synaptic facilitation at presynaptic terminals of the hippocampus upstream of the exocytic machinery.

 $synapse \mid potassium \; channel \mid action \; potential \mid exocytosis \mid synaptic \\ plasticity$

The action potential (AP) firing pattern or "spike code" as typically measured from the soma is a gold standard for neural excitability within circuits. However, at presynaptic terminals the quantitative relationship between the input AP spike code and the magnitude of exocytosis, or vesicle fusion events per AP, can change dynamically as a result of stimulation frequency or firing pattern. Increased firing frequency can significantly increase the number of vesicles that fuse from an identical number of APs. This phenomenon is known as short-term synaptic facilitation, which can significantly enhance information transfer at synapses influencing several aspects of learning and memory (1). Thus, it is important to completely understand the underlying molecular and cellular mechanisms of synaptic facilitation.

A critical initial step in exocytosis is the arrival of AP_{syn} at boutons, whose waveform can exhibit plasticity based on firing frequency. Repetitive firing may cause inactivation of axonal voltage-gated sodium (Na_v) channels and voltage-gated potassium (K_v) channels that control the depolarization and hyperpolarization of the waveform, respectively. K_v inactivation primarily leads to an increase in AP width or broadening (2–9). The width of the AP_{syn} controls the fraction of time that Ca²⁺ channels open and the driving force of Ca²⁺ entry (10). These changes in voltage kinetics during the AP_{syn} will also impact the shape or profile of the Ca²⁺ microdomain envelope that builds locally around open Ca²⁺ channels in the terminal (11, 12). The highly nonlinear influence of Ca²⁺ on exocytosis (13, 14) thus dictates that modest AP_{syn} broadening has the potential to critically impact synaptic facilitation (15–17). Indeed, AP_{syn} broadening during repetitive firing has been demonstrated to cause the facilitation of exocytosis in the pituitary nerve (3), dorsal root ganglion (18), and mossy fiber bouton (2), all due to K_v channel inactivation. However, the AP_{syn} waveform in Purkinje cells has also been shown to undergo

frequency-dependent decreases in amplitude that substantially contribute to synaptic depression (19). Thus, it is best to consider the AP_{syn} as a plastic signal that can powerfully modulate exocytosis bidirectionally, rather than as a digital spike acting solely as an initiation signal. We therefore reason that the somatic AP has proven to be a poor predictor of exocytosis magnitude as a result of a failure to resolve the AP_{syn} waveform and its molecular regulators in the majority of brain regions.

As opposed to the majority of larger synapses, en passant terminals are most commonly involved in brain regions associated with synaptic plasticity. Investigating the molecular regulation of AP_{syn} in the common en passant nerve terminals of the cortex and hippocampus remains elusive due to the small size of these structures (<1 µm), which makes them inaccessible for whole-cell patch clamp recording. An innovative initial strategy to overcome these size restrictions was the use of voltage dyes, which failed to detect use-dependent changes in the AP_{syn} in hippocampal slices (20). However, these dyes were limited by very low voltage sensitivity (<0.5% change in fluorescence for an AP) requiring population averaging, and these dyes were unable to report a stable resting voltage during stimulation (20). Moreover, it was found only later that this class of voltage dyes were phototoxic and altered membrane physiology, limiting their usefulness in small axons (21). As a result of these complications, the question of AP_{syn} plasticity as a modulator of synaptic

Significance

Nerve terminals generally engage in two opposite and essential forms of synaptic plasticity (facilitation or depression) that play critical roles in learning and memory. While the molecular components of both types of terminals are similar with regards to vesicle fusion, much less is known about their molecular control of electrical signaling. Measurements of the electrical impulses (action potentials) underlying these two forms of plasticity have been difficult in small nerve terminals due to their size. In this study we deployed optical physiology measurements to overcome this size barrier. Here, we identify a unique mechanism (Kv β 1 subunit) that enables broadening of the presynaptic action potentials that selectively supports synaptic facilitation, but does not alter any other aspects of nerve terminal function.

Author contributions: I.H.C., M.C., G.E.O., R.A.H., and M.B.H. designed research; I.H.C., L.C.P., S.A.A., R.A.H., and M.B.H. performed research; I.H.C., L.C.P., M.C., S.A.A., G.E.O., R.A.H., and M.B.H. analyzed data; and I.H.C. and M.B.H. wrote the paper.

The authors declare no competing interest.

This article is a PNAS Direct Submission.

This open access article is distributed under Creative Commons Attribution-NonCommercial-NoDerivatives License 4.0 (CC BY-NC-ND).

¹Present address: Program in Neuroscience, Harvard University, Cambridge, MA 02138.

²To whom correspondence may be addressed. Email: michael.b.hoppa@dartmouth.edu.

 $This article contains supporting information online at \ https://www.pnas.org/lookup/suppl/doi:10.1073/pnas.2000790117/-/DCSupplemental.$

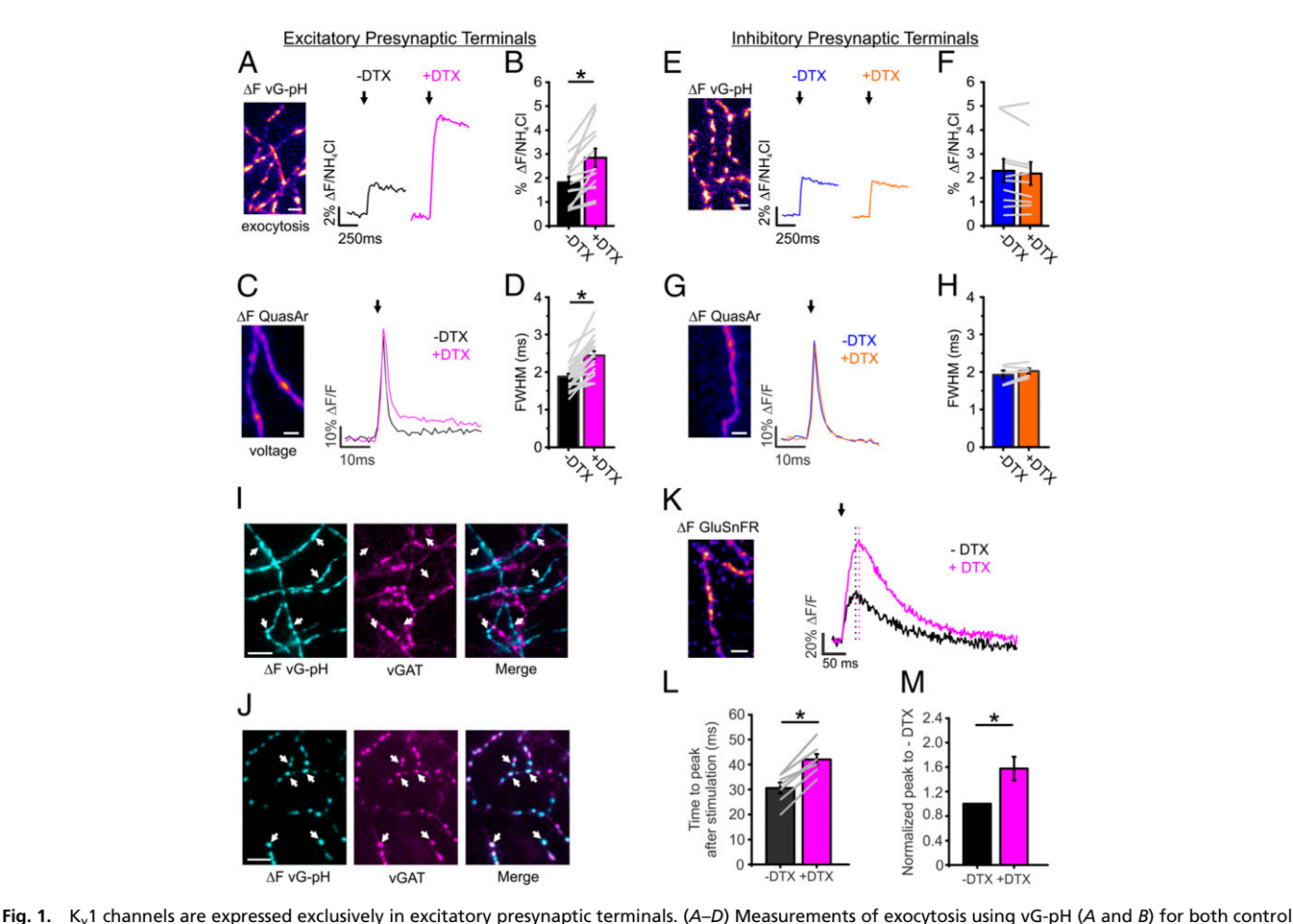
First published November 9, 2020.

Downloaded at Dartmouth College on June 1, 2021

facilitation remains unanswered for hippocampal neurons. Our group has overcome the size barrier of hippocampal axons, while also avoiding cell population averaging and dye toxicity by pioneering the use of genetically encoded rhodopsin-based voltage indicators. Here, we measure the AP_{syn} of individual en passant terminals from both inhibitory and excitatory hippocampal neurons. These measurements demonstrate a striking contrast between facilitating excitatory and depressing inhibitory nerve terminals in the hippocampus. We discovered that excitatory axons and terminals are uniquely enriched with a combination of $K_v 1.1/1.2$ heteromers and $K_v \beta 1$ subunits. This combination of K_v subunits causes rapid AP_{syn} broadening during brief periods of high-frequency firing. This broadening was essential for enabling synaptic facilitation without altering initial exocytosis. We also found that simply overexpressing this K_νβ1 subunit made inhibitory neurons switch from depressing during high-frequency stimulation to facilitation. Taken together, these results suggest that the molecular control of presynaptic K_v channel inactivation is an important modulator of synaptic facilitation upstream of vesicle release machinery.

Results

Previously, our measurements of the AP_{syn} in cultured hippocampal neurons found a very high ratio of K_v to Na_v channels with $K_v 1.1/1.2$ channels dominating repolarization (22), similar to in vivo measurements from CA3 neurons (23). We measured the sensitivity of exocytosis to changes in K_v1.1/1.2 conductance using an optical probe of exocytosis (vGLUT1-pHluorin; vG-pH) (14, 24). Blockade of K_v1.1/1.2 channels by application of dendrotoxin (DTX) greatly enhanced exocytosis in excitatory hippocampal nerve terminals by $61 \pm 18\%$ when stimulated with 1 AP (Fig. 1 A and B). The sensitivity of exocytosis to DTX application was mirrored in the optical recordings of the AP_{svn} from neurons expressing the indicator QuasAr (25) with a characteristic broadening as measured by the full width at half max (FWHM) of the waveform (30 \pm 4%) (Fig. 1 C and D) in agreement with previous findings (22). We measured this phenomenon in both excitatory and inhibitory neurons of the hippocampus without prior knowledge of their identity. Interestingly, the inhibitory neurons did not display any sensitivity to DTX treatment as assayed by exocytosis (Fig. 1 E and F). Furthermore, the AP_{syn} waveform displayed no changes in amplitude or width from DTX treatment (Fig. 1 G and H). We note



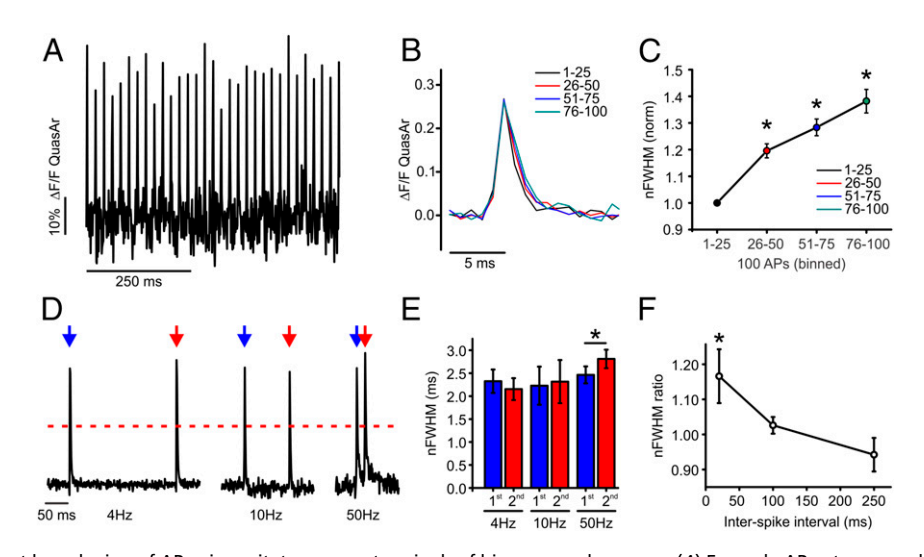
(black) and DTX-treated (magenta) excitatory neurons; arrows indicate when stimulation was applied. Example of recording of voltage using QuasAr (C) and corresponding FWHM (D). (Scale bar, 10 μ m.) (vG-pH, n = 16 cells, *P < 0.001, paired t test; QuasAr, n = 20 cells, *P < 0.01, paired t test). (E-H) Measurements of exocytosis using vG-pH (E and F) in control (blue) and DTX-treated (orange) inhibitory neurons. Representative recording of voltage using Quasar (G) and the corresponding averaged FWHM (H). Arrow in G indicates when stimulation was applied (vG-pH, n = 10 cells; QuasAr, n = 5 cells). (I and I) Representative images of vGAT antibody live staining in excitatory terminals (I) and inhibitory terminals (I). Colocalization of vGAT-staining signal with active synapses marked by vG-pH response is indicated by the white arrows. (Scale bar, 10 μ m.) (I) Representative I0 image of GluSnFR upon single stimulation. Average trace of GluSnFR for both control (black) and DTX-treated (magenta) excitatory neurons; arrow indicates when stimulation was applied; black dotted line indicates the peak of control, and magenta dotted line indicates the peak of DTX-treated neurons, showing the latency (I1 images of test). (I2 cand I3 image) (I3 and I4 image). (I4 and I5 images of the corresponding averaged time to peak after stimulation (I4) and normalized peak to control (I6) are shown. (I8 corresponding averaged time to peak after stimulation (I6) and normalized peak to control (I6) are shown. (I8 corresponding averaged time to peak after stimulation (I6) and normalized peak to control (I7) are shown. (I8 corresponding averaged time to peak after stimulation (I8 and normalized peak to control (I8) are shown. (I8 corresponding averaged time to peak after stimulation (I8 and normalized peak to control (I8 and I8 in the stimulation (I8 an

that QuasAr's reporting of voltage is linear and the most rapid voltage indicator to date; nonetheless, QuasAr has a sampling delay of ~300 μs for changes in voltage as previously demonstrated (25, 26). As a result of this inherent filtering of the reporter, the peak is reduced compared to electrophysiological recordings, and measurements of FWHM will systematically appear broader. However, as QuasAr's delay is uniform in combination with its linear sensitivity to voltage across a large physiological range (±100 mV), it has been shown to comparatively display relative voltage changes in vitro and in vivo with high fidelity in neurons (25-27). We confirmed the identity of neurons after measuring exocytosis or AP_{syn} waveform as excitatory or inhibitory using a fluorescent antibody directed against the luminal domain of the vesicular GABA transporter (vGAT) as previously described (28) with examples for both cell types shown in Fig. 1 I and J. Previously, it has been demonstrated that broadening the AP_{syn} by blocking K_v channels introduces a latency in synaptic transmission (29). We used a fast variant of the glutamate sensor GluSnFR to study the kinetics of glutamate release during AP broadening by DTX treatment and found that indeed the peak of GluSnFR was delayed by 40 ± 6% relative to field stimulation, while also exhibiting a 57 ± 16% increase in neurotransmitter release in good agreement with previous measurements (Fig. 1 K-M). Taken together, these experiments demonstrate a very selective enrichment of presynaptic K_v1 channels in excitatory nerve terminals of hippocampal neurons.

We hypothesized that terminals enriched with $K_v1.1/1.2$ channels might exhibit AP_{syn} broadening during high frequency (>10 Hz) stimulation due to K_v1 channel inactivation. We observed a robust (39 \pm 4%) broadening during a train of stimulation with 100 APs stimulated at 50 Hz (Fig. 2A), with example binned recordings of the AP_{syn} shown in Fig. 2B and the corresponding quantifications of the FWHM in Fig. 2C. Next, we examined if AP_{syn} broadening also took place in short paired-pulse stimulation protocols associated with synaptic facilitation. We measured the FWHM of the AP_{syn} waveform during paired-pulse stimulation to compare how stable the shape of the waveform is across basal firing rates (4 to 10 Hz) and those typically associated with facilitation (50 Hz) (30, 31) (Fig. 2 D

and E). The FWHM paired-pulse ratio (PPR) is plotted as a function of the interspike interval in Fig. 2F, demonstrating that AP_{syn} broadening is reliably triggered by stimulation frequencies of 50 Hz. This broadening behavior for the AP_{svn} during pairedpulse stimulation was exclusive to excitatory terminals and was not seen in inhibitory terminals that exhibited a strong hyperpolarization (12 of 17 neurons; SI Appendix, Fig. S1). When we measured the FWHM of each spike individually during pairedpulse stimulation for both inhibitory and excitatory nerve terminals, we noticed that the broadening at 50 Hz was prominent only in excitatory nerve terminals and absent in inhibitory terminals (SI Appendix, Fig. S1 A, B, E, and F). However, the measurement of individual spikes from their independent baselines failed to account for important changes in voltage for the second AP from the optical voltage recordings, particularly with respect to hyperpolarization. As such, we used the amplitude of the FWHM from the first AP to measure the FWHM for all subsequent recordings to account for absolute changes in voltage that are more relevant to considering the opening time for voltage-gated Ca2+ channel behavior. Measurements based on the half-max of the first AP that account for this hyperpolarization demonstrate a significant narrowing of the APsyn in inhibitory neurons during paired-pulse stimulation at 50 Hz, while also accounting for AP broadening in excitatory neurons (SI Appendix, Fig. S1 C-H). We will refer to this measurement from here on as a normalized FWHM (nFWHM). Taken together, these results suggest that presynaptic terminals enriched with K_v1.1/1.2 channels undergo frequency-dependent broadening of the AP_{syn} even in minimal conditions of paired-pulse stimulation, which could influence vesicle fusion.

We created bicistronic expression vectors to measure voltage paired with Ca^{2+} (Fig. 3 A and B) in single nerve terminals. These measurements had limited signal to noise under such restrictions, but even in the presence of GCaMP, voltage measurements demonstrated robust $\operatorname{AP}_{\operatorname{syn}}$ broadening during paired-pulse (50 Hz) stimulation (Fig. 3 C–G). We found that the width of the first AP was correlated with the magnitude of Ca^{2+} entry at the single AP level (Fig. 3H). However, under paired-pulse



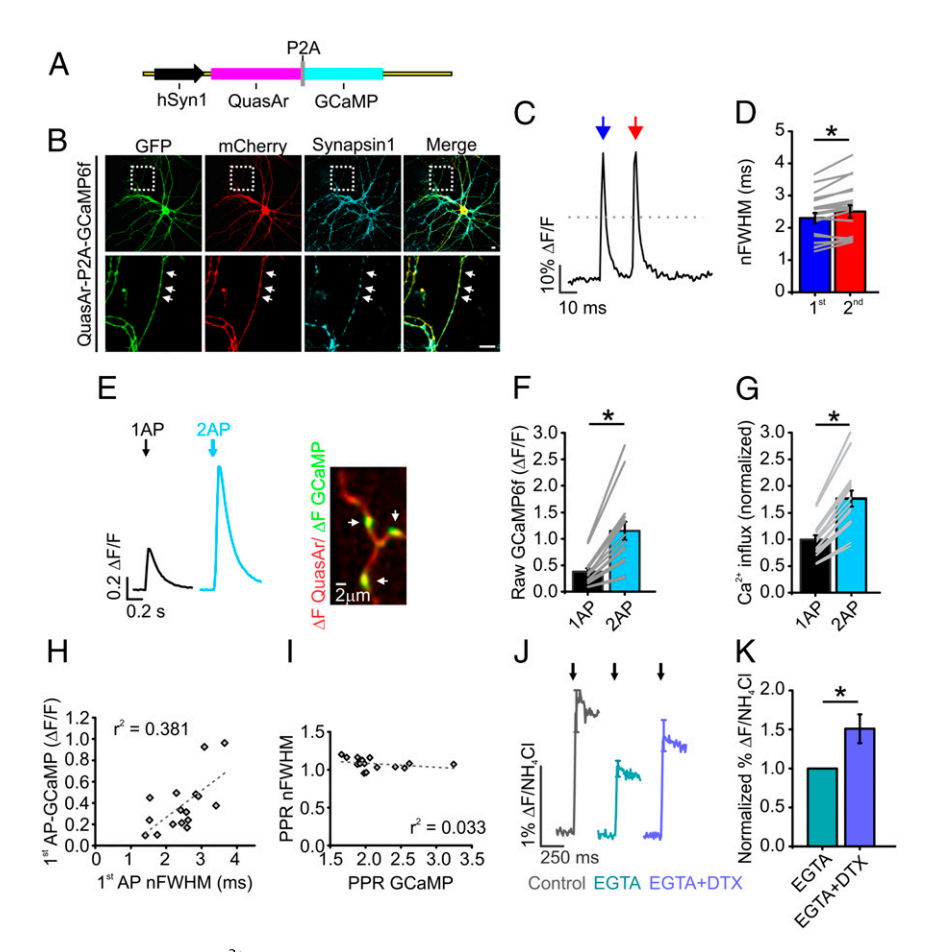


Fig. 3. AP_{syn} broadening alters the profile of Ca^{2+} entry into synaptic terminals. (*A*) Schematic of vector describing bicistronic expression of QuasAr and GCaMP separated by a P2A peptide that cleaves the two proteins for separate localization. (*B*) Immunofluorescence of QuasAr-P2A-GCaMP expression in axons. GCaMP and QuasAr were stained with anti-GFP and anti-mCherry antibodies, respectively. QuasAr contains a nonfluorescent form of the mOrange-tag to prevent cross talk with the GFP signal. Synapsin1 staining was used for marking presynaptic terminals (marked by arrows). (Scale bar, 10 μm.) (*C*) Representative measurement of QuasAr from the axon of an excitatory neuron with en passant synapses with 2 APs at 50-Hz stimulation. Blue arrow indicates the second stimulation. Gray dotted line represents the half maximum where the width was measured. (*D*) Average nFWHM for the first (blue) and second (red) AP waveforms in paired-pulse stimulation of excitatory neurons (n = 19, *P < 0.001, paired t test). Error bars indicate mean ± SEM. (*E, Left*) Representative trace of GCaMP response to a single AP (black) and paired-pulse stimulation (cyan). (*E, Right*) Representative image of QuasAr ΔF (red) and GCaMP ΔF (green) during the stimulation. (Scale bar, 2 μm.) (*F*) Average GCaMP fluorescence in response to a single AP (black) and paired-pulse stimulation (cyan) (n = 16 individual cells). (*G*) Average change in Ca^{2+} as measured by converting GCaMP fluorescence to relative changes in Ca^{2+} to account for the nonlinearity of the GCaMP (*Materials and Methods*) (n = 16 individual cells), *P < 0.001, paired t test. (P < 0.001, paired t test. (P < 0.001) and inference to relative changes in Ca^{2+} influx and nFWHM of first AP-induced Ca^{2+} influx and nFWHM of first AP- Linear fit is shown using a dashed line. (P < 0.001) Correlation between paired-pulse ratio of GCaMP (PPR GCaMP) and nFWHM (PPR nFWHM) using a linear fit. (P < 0.001) Measurements of exocytosis using vG-pH f

stimulation, the PPR for GCaMP (Fig. 3I) was not correlated with the PPR of the AP_{syn} nFWHM. We suspect that these subtle changes were too small for detection by GCaMP6F whose relatively high affinity is best at detecting bulk changes in slow Ca²⁺ transients and not in the local Ca²⁺ where microdomains can collapse quickly (32, 33). Indeed, no indicator or measurement can tell the difference if the number of channels that open or close with different fluxes during changing voltage commands that total calcium could be the same, but the localized microdomains that influence vesicle fusion could be altered dramatically. We suspected that the most significant changes to Ca²⁺ influx during AP_{syn} broadening with respect to influencing vesicle fusion occurs at the level of the Ca²⁺ microdomain profile. As no genetically encoded Ca²⁺ indicators can be localized to detect these changes, we probed the influence of Ca²⁺ microdomains using Ca²⁺ buffers and vG-pH, our sensitive indicator of vesicle fusion. The high-affinity intracellular ethylene glycol tetraacetic

acid (EGTA) molecules strongly restrict Ca^{2+} diffusion to within the microdomain and prevent global diffusion (12, 34). Thus, DTX sensitivity would be diminished after EGTA treatment only if slow changes in Ca^{2+} diffusion outside of a microdomain were responsible for enhanced vesicle fusion instead of changes to the microdomain profile. We found that, while EGTA loading inhibited vesicle fusion by half as compared to control conditions, as previously reported (35), this buffering was quite ineffective in blocking a 50% increase in vesicle fusion after DTX treatment as shown in Fig. 3 J and K. The finding that DTX enhancement to vesicle fusion persisted in the presence of EGTA suggests that Ca^{2+} entry and vesicle fusion are likely to be largely regulated at the level of the Ca^{2+} microdomain by $\operatorname{AP}_{\text{syn}}$ broadening, as long as overall changes in cytosolic Ca^{2+} are small, as when brief stimulation such as paired-pulse is applied.

While many changes in ionic conductances could underlie the rapid broadening of the AP_{syn} during stimulation, the most

suggestive possibility from the previous experiments was that frequency-dependent K_v1.1/1.2 channel inactivation was responsible for broadening. The dominant mechanism of K_v1 family channel inactivation is the "ball-and-chain" mechanism, in which the N-terminal structures of either the K⁺ channel's α- or β- subunits occlude the channel pore from the cytosol (36–38) (Fig. 4A). K_v1.1/1.2 channels are known to most prominently undergo inactivation when associated with cytosolic β- subunits (39). As such, we investigated the role of the $K_v\beta 1$ subunit for AP broadening using short hairpin RNA (shRNA) (Fig. 4 B and C). We verified previous reports (7, 23, 40) of K_v1.1 expression and function in the axons of the hippocampus in vivo using immunohistochemical staining in brain slices. K_v1.1 channels are strongly expressed throughout the hippocampus including the axonal Schaffer collaterals, supporting their role in neurotransmission (Fig. 4 D and E). Next, to explore the physiological role of these channels, we combined shRNA targeting the $K_{\nu}\beta 1$

subunits with QuasAr to determine the involvement of K_v1.1/1.2 inactivation through the β-subunit in the broadening of the AP_{syn} during paired-pulse stimulation. The average waveforms are shown for excitatory neurons expressing scrambled shRNA (wild type [WT]; Fig. 4F) or shRNA directed against K_vβ1 (β1KD; Fig. 4G). We also combined K_vβ1 KD with expression of a human variant of K_νβ1 to rescue KD expression levels and check for off-target effects of KD (+hK_νβ1; Fig. 4H). Genetic depletion of K_vβ1 not only stopped AP broadening, but also caused a small amount of narrowing ($-7.0 \pm 2.6\%$ in the nFWHM) compared to control and rescue terminals ($\pm 10.4 \pm 4.1\%$ and $+8.9 \pm 2.6\%$, respectively, in the nFWHM) (Fig. 4I). This decrease in nFWHM was accompanied by a more prominent hyperpolarization in KD neurons (Fig. 4 F-H) and an overall relative decrease (\sim 11%) in presynaptic AP amplitude (Fig. 4J), suggesting an enhancement of presynaptic K_v1 currents when $K_v\beta 1$ was not expressed. Furthermore, blocking the $K_v 1.1/1.2$

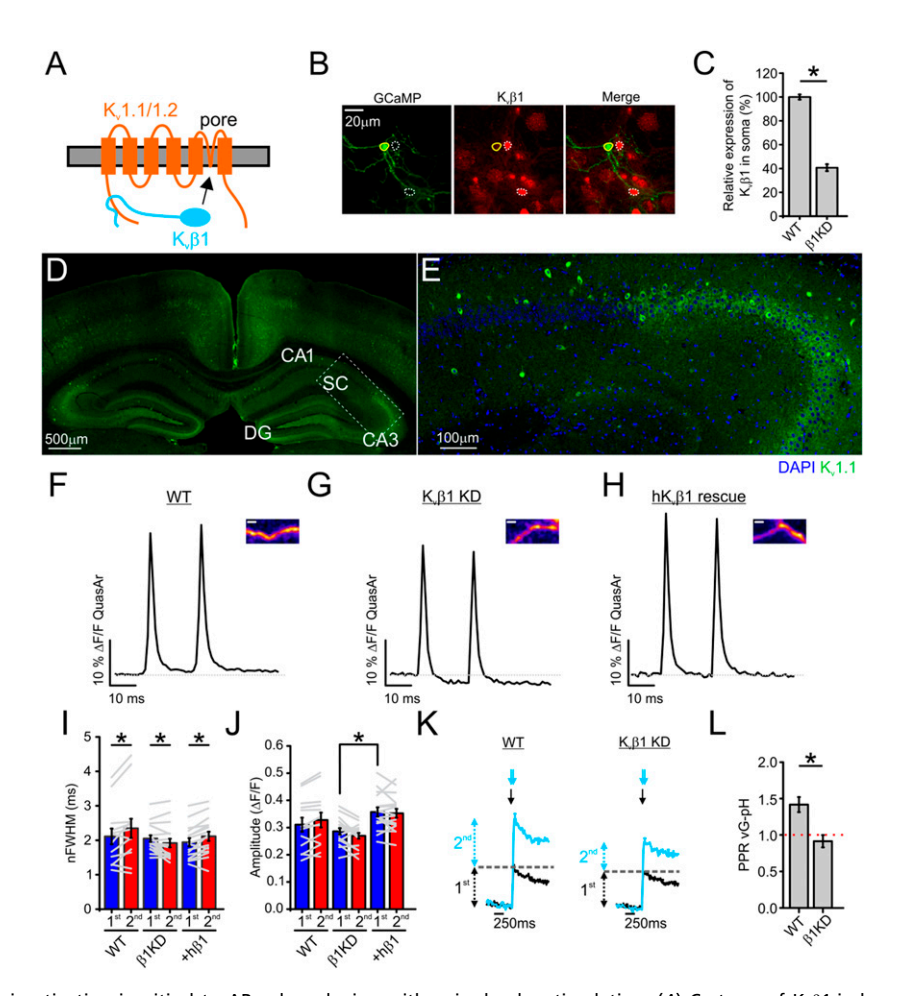


Fig. 4. K_{ν} β1-induced K_{ν} 1 inactivation is critical to AP_{syn} broadening with paired-pulse stimulation. (*A*) Cartoon of K_{ν} β1-induced inactivation of K_{ν} 1.1/1.2 complexes. (*B*) Immunofluorescence staining for GCaMP (using anti-GFP antibody) and endogenous K_{ν} β1 in primary cultured hippocampal neurons. Solid circles indicate the soma of a neuron cotransfected with GCaMP and K_{ν} β1 shRNA, and dashed circles indicate those of untransfected neurons. (Scale bar, 20 μm.) (*C*) Quantification of relative expression of K_{ν} β1 in soma of K_{ν} β1 shRNA transfected neurons compared with WT neurons (n = 50 for control; n = 19 cells for K_{ν} β1 shRNA transfected neurons; *P < 0.001, Student's t test). (D and E) Immunohistochemical staining of adult mouse brain slices with antibodies against K_{ν} 1.1 channels (green) and the nuclear marker DAPI (blue). (*Inset* in D) The transition into the CA1 region where Schaffer collateral (SC) axons are prominent with magnification of *Inset* shown in E. DG: dentate gyrus; CA1 and CA3: regions of the hippocampus. (F and F) Average traces of AP waveforms in response to 2 AP at 50-Hz stimulation from control (F), K_{ν} β1 KD (G), and K_{ν} β1 rescue (H) neurons. *Insets* provide a representative QuasAr ΔF image from each condition. (Scale bar, 2 μm.) (I and I) Average nFWHM (I) and amplitude (I) for the first (blue) and second (red) AP waveform as shown in F-H (WT, I) = 13 cells; K_{ν} β1 KD, I0 = 17 cells; K_{ν} β1 rescue, I1 = 18 cells; I1 cells; I2 the I3 cells; I3 cells; I4 cells; I5 cells; I6 cells; I7 cells; I8 cells; I8 cells; I8 cells; I9 cells; I1 cells cells; I1 cells; I1 cells; I2 cells; I3 cells; I4 cells cells; I5 cells cells; I7 cells; I8 cells cells; I8 cells; I8 cells; I9 cells; I1 cells; I2 cells; I3 cells; I4 cells cells; I5 cells cells; I7 cells cells

isoforms of K_v1 using DTX inhibits AP broadening in both WT and K_νβ1 KD neurons during paired-pulse stimulation at 50 Hz (SI Appendix, Fig. S2), supporting the argument that the inactivation of the K_v1 channel, and not the addition of other K_v channels, is responsible for the phenotype that we measured. We used vG-pH to investigate the consequences of these changes in AP_{syn} broadening on the facilitation or depression of exocytosis during 50-Hz paired-pulse stimulation (Fig. 4K). We found that control (WT) terminals displayed a 42 ± 10% increase in exocytosis (paired-pulse ratio of vG-pH is 1.42; facilitation >1) when comparing stimulation from paired pulses at 50 Hz to a single AP, but this enhancement or facilitation in vesicle fusion was completely abolished in $K_v\beta 1$ KD neurons (-9 \pm 8%; Fig. 4L). We found that inhibitory nerve terminals mimicked the excitatory K_vβ1 KD terminals and exhibited paired-pulse narrowing of the AP_{syn} (SI Appendix, Fig. S3 A and B). We were curious about whether the inhibitory nerve terminals that exhibited narrowing displayed facilitation or depression. We found that this AP_{syn} narrowing was accompanied by depression of neurotransmission (vG-pH ratio <1), akin to $K_{\nu}\beta 1$ KD excitatory neurons (SI Appendix, Fig. S3 C and D). Taken together, these results indicate that $K_{\nu}\beta 1$ subunits play a critical role in AP broadening in excitatory nerve terminals during paired-pulse stimulation and suggest an important modulatory role for presynaptic K_v1.1/1.2 currents in facilitating glutamate release.

The impaired response during 50-Hz paired-pulse stimulation for cells lacking K_νβ1 as reported by vG-pH measurement suggested a selective impairment in facilitation. We attempted to further validate this selective impairment in exocytosis using an imaging technique that directly quantifies glutamate release at various stimulation frequencies of paired-pulse stimulation as a complement to our vG-pH results that measured the exocytosis of synaptic vesicles. To this end, we used the ultrafast variant of the genetically encoded glutamate sensor (iGluSnFR S72T; K_d $600 \,\mu\text{M}$ and K_{off} of $468 \,\text{s}^{-1}$ for glutamate) previously validated in hippocampal slice (41). We found that this GluSnFR variant was rapid enough to resolve glutamate release at 50 Hz (Fig. 5 A–C). While control neurons exhibited a 31% increase in the pairedpulse ratio of glutamate release when comparing stimulation at 50 to 10 Hz for control cells, there was no increase in the pairedpulse response of K_νβ1 KD neurons, as shown in Fig. 5D, consistent with our vG-pH results. Thus the ability to exhibit frequency-dependent facilitation during paired-pulse stimulation was lost with knockdown of the K_νβ1 subunit, but otherwise release seemed to be normal for lower frequencies.

Hippocampal neurons typically fire in short bursts of APs during physiological conditions (42), so we next examined the contribution of K_νβ1-mediated K_ν1.1/1.2 inactivation during synaptic transmission consisting of 10 electrical pulses delivered at 4 or 50 Hz. We found that WT neurons displayed robust facilitation at 50-Hz stimulation (Fig. 6A). However, we observed no facilitation for K_vβ1 KD neurons, despite nearly identical vesicle exocytosis at 4-Hz stimulation compared to WT neurons, suggesting a selective impairment in facilitation (Fig. 6B). Even under an extended protocol of 50 APs delivered at 50 Hz, no recovery was seen in exocytosis (SI Appendix, Fig. S4) in K_νβ1 KD neurons. We found that frequency-dependent synaptic facilitation in neurons overexpressing (OE) hK_vβ1 was no greater than that which we had observed in control neurons (Fig. 6 C and D). Critically, the magnitude of vesicle fusion elicited by a single AP in all conditions was not altered by the loss of $K_{\nu}\beta 1$ nor was any impairment observed for stimulation of a train at 4 Hz. These results suggest that release probability and the vesicle fusion machinery are intact, but that the AP_{syn} itself is a major modulator of facilitation or depression. While many factors could influence facilitation, we also looked more closely at inhibitory neurons, which typically failed to facilitate and are quite stable with regard to vesicle fusion per AP at any frequency.

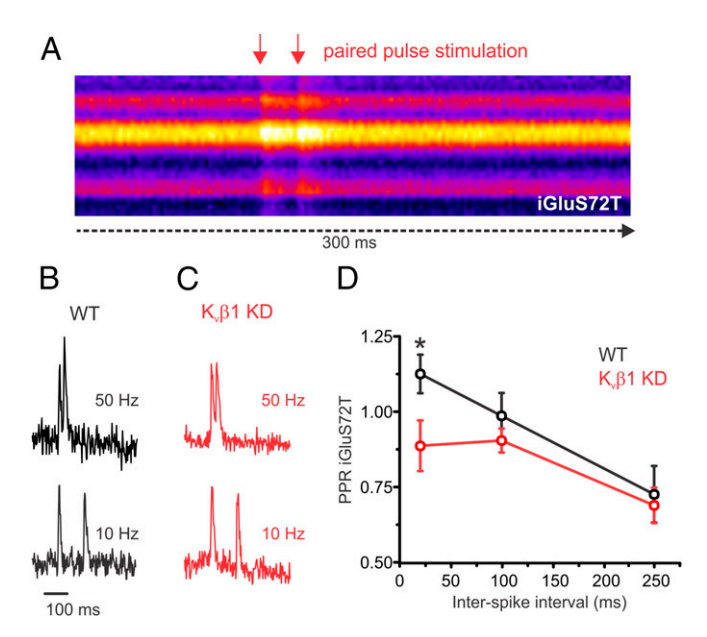


Fig. 5. Paired-pulse measurements of glutamate release is impaired in $K_\nu\beta1$ KD neurons. Optical measurements of glutamate release from individual presynaptic terminals expressing ultrafast iGluSnFR S72T during paired-pulse stimulation at various frequencies. (A) Kymograph of a representative recording across the axon of a hippocampal neuron recorded at 500 Hz and stimulated with a paired-pulse (50 Hz). Representative individual recordings of iGluSnFR S72T for a control (*B*) and $K_\nu\beta1$ KD (*C*) neuron stimulated with 2APs at 50 Hz (*Top*) and 10 Hz (*Bottom*) normalized to the response of the first AP. (*D*) Average iGluSnFR paired-pulse ratio (normalized to glutamate reponse of first AP) from control and $K_\nu\beta1$ KD neurons (control, n=13 cells; $K_\nu\beta1$ KD, n=13 cells; *P<0.05, Student's t test; error bars represent SE). Note the selective impairment of release at 50 Hz compared to 10 and 4 Hz. Extracellular Ca²⁺ concentration is 2 mM in all experiments.

Interestingly, $hK_{\nu}\beta1$ OE alone was able to switch inhibitory neurons into a facilitating state with an ~50% increase in vesicle fusion in the OE inhibitory neurons when increasing the firing frequency from 4 to 50 Hz (Fig. 6 *E–G*). These results argue that the $K_{\nu}\beta1$ subunit alone can initiate facilitation without a need to alter downstream aspects of synaptic terminals such as Ca^{2+} sensing or vesicle fusion.

We also measured the change in the nFWHM of the AP waveform with minimal averaging (16 trials) for both control (WT; gray) and K_νβ1 KD neurons (K_νβ1 KD; orange) for brief trains of 10 AP stimulation at 4 and 50 Hz (Fig. 7 A and B). Here again we found a complete loss of AP_{syn} broadening at 50-Hz stimulation for K_vβ1 KD neurons and a significant narrowing of the AP_{svn} at 4-Hz stimulation (Fig. 7C). While our evidence from paired-pulse stimulation experiments suggests small changes in Ca²⁺ that were mainly confined to the microdomain, we hypothesized that the loss of K_vβ1-mediated broadening of AP_{svn} could also lead to a cumulative overall increase in net Ca²⁺ entry during longer high-frequency stimulation. We tested this hypothesis using a cytosolic version of GCaMP6f and measured changes in presynaptic [Ca²⁺]_i during stimulation with 10 APs at 50 Hz for WT (gray; Fig. 7*D*) and K_νβ1 KD neurons (orange; Fig. 7E). Here we found that the presynaptic Ca^{2+} signal was strongly reduced (>50%) during trains of stimulation at 50 Hz for $K_v\beta 1$ KD neurons (Fig. 7F). As such, these results indicate that minor changes in AP_{svn} broadening by loss of K_vβ1mediated K_v1 inactivation likely have an immediate impact on the Ca2+ microdomain profile, but also can have a large cumulative impact on integrated [Ca²⁺]_i and synaptic facilitation during physiological patterns of activity.

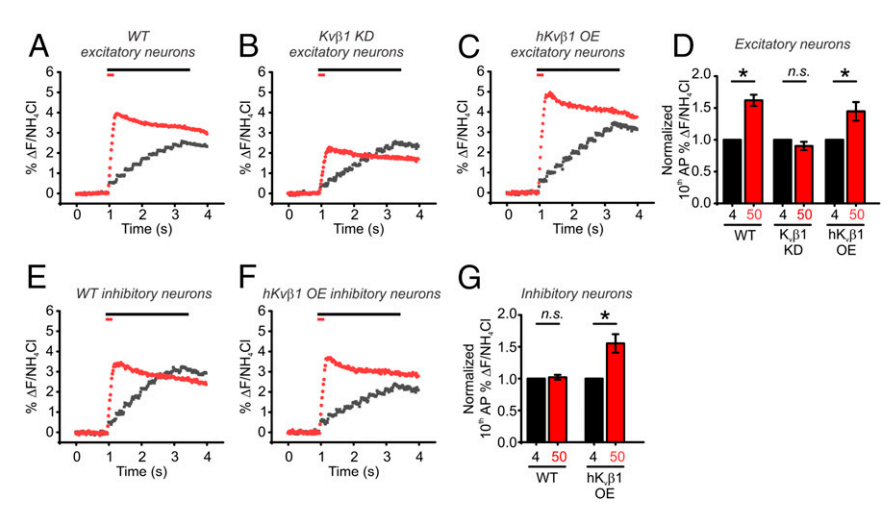


Fig. 6. Synaptic facilitation is absent in $K_{\nu}\beta1$ KD neurons. (A–C) Average traces of pHluorin measurements of exocytosis for WT (A), $K_{\nu}\beta1$ KD (B), and human $K_{\nu}\beta1$ overexpressed (C) excitatory neurons in responses to 10 APs delivered at 4 Hz (black) or 50 Hz (red) as measured with vG-pH. Bars at top of the graphs indicate the duration of each stimulation. (D) Normalization of average fusion induced by the 10th AP as a percentage of total vesicle fluorescences measured by application of NH₄Cl. Neurons were stimulated with 10 AP at 4 Hz (black) or 50 Hz (red) (WT neurons, n = 16 cells; $K_{\nu}\beta1$ KD neurons, n = 8 cells; $K_{\nu}\beta1$ OE neurons, $K_{\nu}\beta1$ CD neurons, $K_{\nu}\beta1$ CD and $K_{\nu}\beta1$ overexpressed ($K_{\nu}\beta1$) inhibitory neurons in responses to 10 APs delivered at 4 Hz (black) or 50 Hz (red) as measured with vG-pH. Bars at top of the graphs indicate the duration of each stimulation. ($K_{\nu}\beta1$) Normalization of average fusion induced by the 10th AP as a percentage of total vesicle fluorescences measured by application of NH₄Cl. Neurons were stimulated with 10 AP at 4 Hz (black) or 50 Hz (red) (WT neurons, $K_{\nu}\beta1$) OE neurons, $K_{\nu}\beta1$ OE neurons, $K_{\nu}\beta1$ os paired $K_{\nu}\beta1$ test). Extracellular Ca²⁺ concentration is 2 mM in all experiments.

Discussion

Our central finding is that an important mechanism of synaptic facilitation in excitatory hippocampal neurons is AP_{syn} broadening. We find that the surprisingly rapid frequency-dependent broadening of AP_{syn} is enabled by a unique molecular combination of $K_v1.1/1.2$ channels with the $K_v\beta1$ subunit. Indeed, this small broadening of the AP_{syn} mediated by $K_v\beta1$ has a tremendous

impact on synaptic transmission as the loss of the $K_v\beta 1$ subunit blocks synaptic facilitation even during paired-pulse stimulation without altering initial vesicle fusion (Figs. 4–6). We believe that the conditions of AP_{syn} broadening work to facilitate exocytosis through a host of additional molecular interactions that minimally include downstream Ca^{2+} sensors and enzymes, but that K_v1 inactivation represents a critical initial step to enable facilitation.

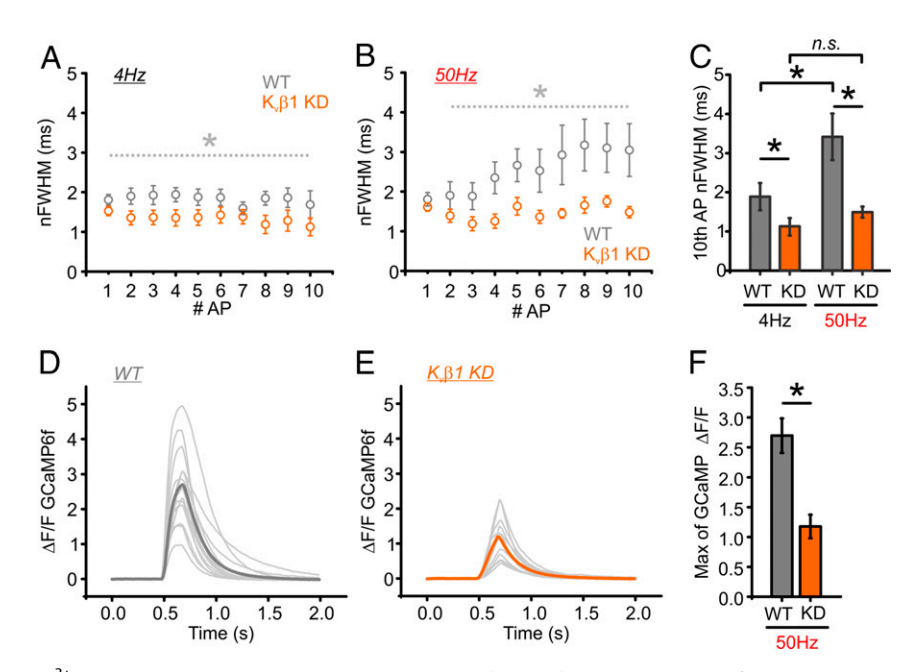


Fig. 7. AP broadening and Ca²⁺ accumulation are inhibited in $K_{\nu}\beta1$ KD neurons. (*A* and *B*) Optical recording of APs in neurons expressing QuasAr stimulated with 10 AP at 4 Hz (*A*) and 50 Hz (*B*). nFWHMs of each AP across the stimulus train from WT (gray) and $K_{\nu}\beta1$ KD (orange) cells are displayed (*n* = 16 trials per cell; WT = 9 cells; $K_{\nu}\beta1$ KD = 7 cells). (*C*) Quantification of the averaged nFWHM of the 10th AP from WT and $K_{\nu}\beta1$ KD (*n* = 9 cells for WT; *n* = 7 cells for $K_{\nu}\beta1$ KD, **P* < 0.05, Student's *t* test). Error bars indicate mean ± SEM. (*D* and *E*) Ca²⁺ influx was measured with GCaMP6f in control (*D*) and $K_{\nu}\beta1$ KD (*E*) neurons. The light gray traces represent individual experiments with the averaged Ca²⁺ influx depicted in dark gray (WT) or orange ($K_{\nu}\beta1$ KD). (*F*) Quantification of the averaged GCaMP6f response of the 10th AP from WT and $K_{\nu}\beta1$ KD neurons (*n* = 14 cells for WT; *n* = 11 cells for $K_{\nu}\beta1$ KD; **P* < 0.001, Student's *t* test). Extracellular Ca²⁺ concentration is 2 mM in all experiments.

This combination of K_v1 isoforms and subunits is not a ubiquitous system, and even in cultured hippocampal inhibitory and excitatory neurons demonstrated substantially different modulation of AP_{syn} and presynaptic K_v isoform enrichment (Figs. 1 and 6 and SI *Appendix*, Fig. S3). Interestingly, the expression of K_v channel isoforms appeared to be one of the larger molecular differences between the synapses of these two neuronal cell types that display such opposite phenotypes in synaptic plasticity. This was demonstrated by simply overexpressing the K_νβ1 subunit, which switched the inhibitory neurons from a depressing to a facilitating phenotype during high-frequency stimulation (Fig. 6 E–G). This result suggested a trafficking role for the $K_{\nu}\beta 1$ subunit in addition to its role in K_v1 inactivation that modulates paired-pulse and frequency-dependent facilitation as we describe here. As such, we believe a detailed accounting of all of the K⁺ channels and subunits responsible for the AP_{syn} shape across axons and associated terminals in various neural cell types could be an important contribution to our understanding of short-term synaptic plasticity and circuit dynamics. While many of the calcium sensors and vesicle release machinery seem to be expressed at nearly ubiquitous levels in these two types of cells, their response to the upstream voltage commands during stimulation could be a major deciding factor for dynamically altering neurotransmitter output during different stimulation frequencies. A central limitation of this study is that high-resolution optical measurement of the AP_{syn} in hippocampal neurons is restricted to in vitro experiments. Nevertheless, we believe this well-studied model for presynaptic function, involving a channel enriched in hippocampal axons in vivo (Fig. 4 D and E), will further our understanding of how the AP_{syn} is involved in short-term plasticity and learning and memory in vivo, as it has been previously reported in the $K_v\beta 1$ knockout mouse (43). Furthermore, our noninvasive optical measurements of voltage did not impact normal release probability of the neurons studied, a drawback of the high-resolution whole-cell electrophysiology that was elegantly applied previously to the large mossy fiber boutons (2). It is unclear in those experiments if this alteration in synaptic properties is a consequence of the strong depolarization of the terminal membrane during electrode approach or a result of cytosolic washout of the terminal (2). Nevertheless, neither occur using rhodopsin-based voltage indicators, allowing rigorous measurements of the APsyn while perfectly preserving the properties of synaptic function to study aspects of synaptic plasticity.

Forms of synaptic enhancement, such as facilitation, augmentation, and posttetanic potentiation, are usually attributed to the effects of a residual elevation in presynaptic [Ca²⁺]_i, acting on one or more molecular targets (44). Synaptotagmin 7 (Syt-7), a critical specialized high-affinity Ca²⁺ sensor (45), was identified as a requirement for facilitation in several regions of the brain including the hippocampus (42). However, subsequent studies found prominent levels of Syt-7 in several other neural cell types that exhibit synaptic depression (46-49). Taken together, these experiments suggest that Syt-7 produces facilitation in coordination with other molecular cascades, which remain to be determined. Our data suggest that part of this coordination can occur upstream of Ca²⁺ sensing and the vesicle release machinery. A widely accepted, but difficult-to-test, model of facilitation attributes the enhancement of exocytosis to residual Ca²⁺ buildup during high-frequency stimulation. En passant terminals like those in the cortex and hippocampus have been shown to have very efficient clearance of Ca²⁺ by diffusion thanks to abundant adjacent axonal volume unlike larger single terminals such as the Calyx of Held and could make alteration to Ca²⁺ dynamics during an AP spike more relevant for driving vesicle fusion (50). These measurements, however, are not trivial. Most measurements of the nonlinear relationship between Ca²⁺ entry and vesicle fusion have relied on changes to extracellular Ca²⁺ with a single-AP stimulus input between conditions

for simplicity that would have the same shaped AP_{syn} (13, 51). However, when extracellular Ca²⁺ is constant, the kinetics of the voltage spike of the AP_{syn} can alter the profile of Ca²⁺ entry thanks to changes in driving force during Ca_v channel opening. Previously, whole-cell electrophysiology recordings from the mossy fiber demonstrated that the K_v1 blockade impairs peak Ca²⁺ entry while enhancing total Ca²⁺ influx (charge) (2). While it should be expected that optical indicators would still identify charge by simply binding more calcium that enters the cytosol, their competition with mobile buffers could complicate total Ca²⁺ detection with different kinetics of entry. In practice, previous optical measurements of synaptic Ca²⁺ during Kv1 blockade in basket cells have failed to detect changes in single-AP stimulation using a high-affinity indicator (52). However, recent experiments with brief trains of stimulation and a lowaffinity indicator in basket cells display a clear change in bulk Ca²⁺ influx (53), which closely matches our own measurements with GCaMP6F (Fig. 7). We also suggest an interpretation that the number of Ca²⁺ channels that open or inactivate during different command voltages could be variable, although this has not been modeled and would be currently difficult to test. In synapses, we still do not know if many open Ca²⁺ channels with smaller single-channel flux might be less effective in driving a response than fewer open channels, each with a larger singlechannel flux, a property that could also be altered by different waveform shapes (12). Our finding (Fig. 3) that strong buffering of Ca²⁺ entry by EGTA loading did not impair the DTX enhancement of vesicle fusion suggests that AP broadening importantly impacts the profile of Ca²⁺ entry specifically at the level of local microdomains at the synaptic terminal. Hopefully, new variants of faster Ca2+ indicators that are genetically encodable and also emit orthogonally to those measuring neurotransmitter release will allow this to be tested in the near future.

A second potential mechanism for this enhancement of intracellular Ca2+ during high-frequency stimulation is activitydependent activation of Ca_v channels (54). However, this does not seem to be relevant in hippocampal neurons at physiological temperatures (55) such as the ones that we used in our experiments. We measured Ca²⁺ in control and K_vβ1 KD neurons and found that substantial buildup of global [Ca2+]i is strongly enhanced by AP_{syn} broadening when measured during physiological trains of stimulation (Fig. 7) that were not measurable during paired-pulse stimulation. We speculate that this is especially critical in light of efficient Ca²⁺ extrusion coupled with the low overshoot (+7 mV) of the excitatory AP_{syn} that will typically open only a fraction of available presynaptic Ca²⁺ channels, a phenomenon that we have previously identified in excitatory terminals of the hippocampus (22). Thus, AP_{svn} broadening may be a particularly efficient mechanism for facilitation in en passant boutons in general.

While we demonstrate that AP_{syn} broadening mediated by K_v1 inactivation is important for facilitation in excitatory hippocampal neurons, we do not believe it is conserved across all terminals as demonstrated by our measurements in inhibitory neurons (SI Appendix, Fig. S3). Interestingly, it appears that, without $K_v\beta 1$ subunits, overall K_v currents are activated during high-frequency stimulation. This lack of inactivation results in significant narrowing of AP_{syn} which was clearly observed for paired-pulse stimulation in inhibitory neurons as well as in K_νβ1 KD excitatory neurons. Presynaptic K_v channel activation during high-frequency stimulation was previously reported in the Calyx of Held (56) and may indeed be the default mode for many presynaptic K_v channels. This activation of K_v channels could be a very useful property for neurons that typically exhibit high firing rates such as hippocampal parvalbumin-expressing inhibitory neurons to depress exocytosis and to maintain a supply of vesicles as well as to preserve the timing of neurotransmitter release. This also seemed to be the case in Purkinje cell terminals

that exhibit frequency-dependent attenuation of AP_{syn} at larger terminals synapsing with deep cerebellar nuclei (19). The mechanisms that activate K_v channels are not fully resolved at present and may involve the recruitment of Ca²⁺-sensitive K⁺ channels such as SK and BK channels. What is clear is that K⁺ channel inactivation during physiological stimulation is not an inherent property of all neurons and that for some K_v1 channels (K_v1.1 and 1.2 heteromers) binding partners are required. Here we identified the $K_{\nu}\beta 1$ subunit as a powerful modulator of exocytosis and synaptic facilitation. K_v1 channel inactivation by the K_vβ subunit is well conserved, with homologs (Shaker and Hyperkinetic) found in Drosophila which act in a similar manner (57). Additionally, impaired inactivation of K_v1 channels was identified as a presynaptic channelopathy of ataxia, which, combined with our findings, suggests K_v inactivation's broad importance across several circuits in the brain (58). As previous behavioral experiments in K_vβ1 knockout mice have identified the $K_{\nu}\beta 1$ subunits as being critical for many memory tasks (43), we believe that our findings may be helpful for understanding the mechanism underlying this phenotype. Previous slice recordings in this knockout mouse did not show impaired facilitation. However, we point out that a critical difference between these measurements and ours was that the recordings in slice were performed at room temperature, while ours were performed at physiological temperatures (>34 °C). Additionally, while $K_{\nu}\beta 1$ subunits seem critical for frequency-dependent inactivation, other mechanisms or even subunits may also be involved through different analog voltage signals in the axon (17, 23). We believe our data provide evidence that the AP_{syn} waveform is a critical modulator of synaptic facilitation in excitatory nerve terminals and that further study of presynaptic K⁺ channels is warranted across neuronal cell types.

Materials and Methods

Cell Culture and Transfection. Primary hippocampal neurons from postnatal day 1 Sprague–Dawley rats of either sex were cultured by dissociation from newborn rat pups. Briefly, hippocampal CA1-CA3 regions were digested with trypsin for 5 min at room temperature and dissociated into single cells. Cells were seeded inside a 6-mm-diameter cloning cylinder on polyornithine-coated coverslips. Plasmids were transfected into 5-to 6-d in vitro (DIV) neurons with Ca²⁺-phosphate precipitants. Male and female C57BL/6J mice (aged 4 to 12 wk) were used and maintained in a temperature- and humidity-controlled animal vivarium at a 12/12 light/dark cycle with food and water provided ad libitum. All animal protocols were approved by Dartmouth College's Institutional Animal Care and Use Committee (protocol number 0002115 for rats and 0002158 for mice). All reagents used can be found in *SI Appendix*, Table S1.

Plasmids. QuasAr (variant DRH 334, Quasar2; hSyn promoter) (25) constructs and vG-pH have been described previously (25, 59). GluSnFR B16 was obtained from Jonathin Marvin, Janelia, Ashburn, VA. The iGluSnFR S72T plasmid was acquired from Addgene (plasmid #106122 variant iGluu) with advice on its use from Thomas Oertner, Center for Molecular Neurobiology, Hamburg, Germany. To measure membrane potential and Ca²⁺ influx in the same cell, we designed a QuasAr-P2A-GCaMP by inserting QuasAr fused to P2A peptide synthesized using GeneArt Gene Synthesis (Invitrogen) and GCaMP6f under the human Synapsin1 promoter, inducing simultaneous expression of two different proteins in neurons. We validated that QuasAr and GCaMP were coexpressed in the same cells through an immunostaining assay and many repetitive experiments. To knock down endogenous $K_{\nu}\beta 1$ expression, shRNA plasmids were obtained from OriGene against the following messenger RNA target sequence: GCTTGGTCATCACAACCAAACTCTACTGG. For rescue experiments in $K_{\nu}\beta 1$ knockdown neurons, human $K_{\nu}\beta 1.1$ fused to a P2A peptide synthesized using GeneArt Gene Synthesis was inserted into the pFCK-QuasAr plasmid to induce independent expression of QuasAr and human $K_{\nu}\beta 1.1$ in neurons. For human $K_{\nu}\beta 1.1$ overexpression experiments, we designed a mOrange-P2A-human $K_{\nu}\beta 1.1$ under the human Synapsin1 promoter, inducing simultaneous expression of two different proteins in neurons.

Antibodies and Reagents. Chicken polyclonal anti-GFP and rabbit polyclonal anti-mCherry were purchased from Invitrogen. Rabbit polyclonal anti-VGAT-Alexa 550 and mouse monoclonal anti-Synapsin1 were obtained from Synaptic Systems.

Mouse monoclonal anti- K_{ν}) 1.1 was purchased from Neuromab (K9/40), and mouse monoclonal anti- K_{ν} 1.1 was purchased from Neuromab (K36/15). Alexa Fluor 488-, 546-, and 647-conjugated goat anti-rabbit, anti-mouse, anti-chicken, and anti-guinea pig IgG were obtained from Thermo Fisher Scientific. Dendrotoxin-k and EGTA were purchased from Alomone and Thermo Fisher Scientific, respectively. All reagent details for ordering can be found in *SI Appendix*, Table S1.

Live-Cell Imaging. All live-imaging experiments were set up as previously described (26, 60). Briefly, images were obtained using an Olympus microscope (IX-83) equipped with a 40× 1.35 numerical aperture (NA) oil immersion objective (UApoN40XO340-2) and captured with an IXON Ultra 897 EMCCD (Andor). Coverslips were mounted in a laminar-flow perfusion and stimulation chamber on the stage of the microscope. Cells were perfused continuously at a rate of 400 µL/min in Tyrode solution containing the following (in mM): 119 NaCl, 2.5 KCl, 2 CaCl₂, 2 MgCl₂, 25 Hepes, and 30 glucose with 10 µM CNQX and 50 µM AP5 during experiments. All experiments were performed at 34 to 35 °C with a custom-built objective heater.

For K_v1 channel experiments, DTX was used at 100 nM concentrations. Cells were incubated with DTX in Tyrode solution for 1 min, followed by perfusion with normal Tyrode solution for an additional 1 min, and images were taken.

For measuring membrane potential, fluorescence of QuasAr was recorded with an exposure time of 980 μs , and images were acquired at 1 kHz using an optomask (Cairn Research) to prevent light exposure of nonrelevant pixels. Cells were illuminated by a 637-nm laser 70 to 120 mW (Coherent OBIS laser) with ZET635/20×, ET655lpm, and ZT640rdc filters, all obtained from Chroma. We repeated more than 100 trials to measure axonal AP waveforms and averaged the signals, except 10 AP stimulation results in Fig. 4 (16 trials). Timing of stimulation was delivered by counting frame numbers from a direct readout of the EMCCD rather than time itself for more exact synchronization using an Arduino board and software custom manufactured by Sensorstar.

For measuring Ca²⁺ influx and vesicle fusion, fluorescences of GCaMP6f and vG-pH were collected with an exposure time of 20 ms, and images were acquired at 50 Hz. Cells were illuminated by a 488-nm laser 6 to 8 mW (Coherent OBIS laser) with ET470/40x, ET525/50 m, and T495lpxr filters (Chroma). We repeated more than 16 trials to measure single AP-induced responses and 6 trials to measure AP train stimulation-induced responses.

For measuring glutamate release of single action potentials, fluorescence of venus-GluSnFR B16 was collected with an exposure time of 2 ms, and images were acquired at 500 Hz using an optomask. Cells were illuminated by a 520-nm laser 3 to 5 mW with ZET520/20x ET560/40 m, and T535lpxr filters (Chroma). We repeated 10 trials to measure single AP-induced responses in the absence or presence of DTX. Measurement of glutamate release during paired-pulse stimulation (GluSnFR S72T) was performed using illumination by a 488-nm laser 1 mW (Coherent OBIS laser) with ET470/40x, ET525/50 m, and T495lpxr filters (Chroma) for light collection. Acquisition images were acquired at 500 Hz using an optomask as mentioned above for voltage imaging. Final measurements were made by stimulating three times at each frequencies (4, 10, and 50 Hz) measured from individual neurons (each "n" corresponds to an individual cell).

For differentiating inhibitory neurons from excitatory neurons, live vGAT antibody staining was performed using a fluorescent antibody directed against the luminal domain of vGAT, which becomes exposed to extracellular regions after vesicle exocytosis, at the end of the experiments. In detail, cells are incubated with vGAT antibodies and then stimulated by 1,000 AP at 10 Hz followed by perfusion with normal Tyrode solution for 5 min. During the stimulation, vGAT antibodies bind to vGAT exposed to extracellular regions and are transported into the cells by vesicle endocytosis. Only inhibitory neurons show vGAT staining at synapses. Fluorescence was captured using ET560/40×, ET630/75 m, and T585lpxr filters (Chroma).

EGTA loading was accomplished using an acetoxymethyl ester form (Invitrogen E1219) at a 10-mM concentration in dimethylsulfoxide, diluted 1:100 in Tyrodes buffer and loaded into cells for 5 min on the microscope with temperature maintained at 34 °C. Cells were washed for 10 min prior to measurements.

Fixed-Tissue Imaging. All images from tissue sections were captured on an upright Leica SP8 confocal laser-scanning microscope with $10\times (0.4 \text{ N.A.}$, air) or $63\times (1.40 \text{ N.A.}$, oil) objective lenses with 405- and 488-nm lasers used for fluorophore excitation. Leica HyDs (hybrid detectors) coupled with an acousto-optical beam splitter were used for capturing optimal fluorophore emission.

Immunofluorescence of Cultured Neurons. To confirm the coexpression of QuasAr and GCaMP or vG-pH in the neurons, 14 to 17 DIV neurons were

fixed with 4% paraformaldehyde and 4% sucrose in phosphate-buffered saline (PBS) for 10 min, permeabilized with 0.2% Triton X-100 for 10 min, and blocked by 5% goat serum in PBS for 30 min at room temperature. Cells were then incubated with the appropriate primary antibodies and visualized using Alexa Fluor-conjugated secondary antibodies in the PBS containing 5% goat serum. Images were obtained using a custom-made fluorescence microscope equipped with the 40× oil-immersion objectives and filters described above.

Tissue Processing and Immunohistochemistry. Mice (aged 4 to 12 wk) were anesthetized and perfused with 4% paraformaldehyde, and brains were postfixed overnight at 4 °C. Brain-tissue sections 50 μm thick were cut on a vibratome and processed for immunohistochemistry. Tissue sections were blocked in PBS containing 5% normal goat serum and 0.5% Triton-X-100 at room temperature for 1 h. All primary and secondary antibodies were diluted 1:500 in PBS containing 5% normal goat serum and 0.1% Triton-X-100. Tissue sections were incubated in primary antibodies overnight at 4 °C and secondary antibodies for 1 h at room temperature. Specific antibodies used are listed in *Antibodies and Reagents* above.

Image and Data Analysis. Images were analyzed in ImageJ and Fiji using custom-written plugins (http://rsb.info.nih.gov/ij/plugins/time-series.html). To measure fluorescence of probes accurately, we selected 1.4-µm-diameter circular regions of interest (ROIs) from ΔF images of each experiment, centering over the brightest pixel of the ΔF image using an automated program free of bias by the selector. ROIs were selected on the basis of localized responses of voltage, calcium, or vesicle fusion, rather than on morphology, to define a presynaptic terminal (even though en passant boutons can generally be recognized morphologically by a small swelling). All statistical data are presented as means +/— SEM (n = number of neurons), and all experiments were performed on more than three independent cultures. For examining AP broadening with QuasAr measurement, we used Origin version 9.1. To obtain the nFWHM of each peak, half maximum of the first peak

- S. L. Jackman, W. G. Regehr, The mechanisms and functions of synaptic facilitation. Neuron 94, 447–464 (2017).
- J. R. Geiger, P. Jonas, Dynamic control of presynaptic Ca(2+) inflow by fastinactivating K(+) channels in hippocampal mossy fiber boutons. *Neuron* 28, 927–939 (2000).
- M. B. Jackson, A. Konnerth, G. J. Augustine, Action potential broadening and frequency-dependent facilitation of calcium signals in pituitary nerve terminals. Proc. Natl. Acad. Sci. U.S.A. 88, 380–384 (1991).
- P. W. Liu, N. T. Blair, B. P. Bean, Action potential broadening in capsaicin-sensitive DRG neurons from frequency-dependent reduction of Kv3 current. *J. Neurosci.* 37, 9705–9714 (2017).
- Y. Ma, P. O. Bayguinov, M. B. Jackson, Action potential dynamics in fine axons probed with an axonally targeted optical voltage sensor. eNeuro 4, ENEURO.0146-17.2017 (2017).
- S. Rama, M. Zbili, D. Debanne, Modulation of spike-evoked synaptic transmission: The role of presynaptic calcium and potassium channels. *Biochim. Biophys. Acta* 1853, 1933–1939 (2015).
- S. Rama et al., The role of axonal Kv1 channels in CA3 pyramidal cell excitability. Sci. Rep. 7, 315 (2017).
- M. J. M. Rowan, J. M. Christie, Rapid state-dependent alteration in K_v3 channel availability drives flexible synaptic signaling dependent on somatic subthreshold depolarization. Cell Rep. 18, 2018–2029 (2017).
- L. R. Shao, R. Halvorsrud, L. Borg-Graham, J. F. Storm, The role of BK-type Ca2+dependent K+ channels in spike broadening during repetitive firing in rat hippocampal pyramidal cells. J. Physiol. 521, 135–146 (1999).
- B. P. Bean, The action potential in mammalian central neurons. Nat. Rev. Neurosci. 8, 451–465 (2007).
- E. Neher, Vesicle pools and Ca2+ microdomains: New tools for understanding their roles in neurotransmitter release. Neuron 20, 389–399 (1998).
- A. B. Parekh, Ca2+ microdomains near plasma membrane Ca2+ channels: Impact on cell function. J. Physiol. 586, 3043–3054 (2008).
- F. A. Dodge Jr, R. Rahamimoff, Co-operative action of calcium ions in transmitter release at the neuromuscular junction. J. Physiol. 193, 419–432 (1967).
- P. Ariel, M. B. Hoppa, T. A. Ryan, Intrinsic variability in Pv, RRP size, Ca(2+) channel repertoire, and presynaptic potentiation in individual synaptic boutons. Front. Synaptic Neurosci. 4, 9 (2013).
- B. L. Sabatini, W. G. Regehr, Control of neurotransmitter release by presynaptic waveform at the granule cell to Purkinje cell synapse. J. Neurosci. 17, 3425–3435 (1997).
- J. G. Borst, F. Helmchen, Calcium influx during an action potential. *Methods Enzymol.* 293, 352–371 (1998).
- M. Zbili, D. Debanne, Past and future of analog-digital modulation of synaptic transmission. Front. Cell. Neurosci. 13, 160 (2019).
- D. Park, K. Dunlap, Dynamic regulation of calcium influx by G-proteins, action potential waveform, and neuronal firing frequency. J. Neurosci. 18, 6757–6766 (1998).

was applied to every peak. For analyzing vesicle fusion of each condition, the delta response of pHluorin fluorescence was normalized to the change in fluorescence from the total number of vesicles in the synapse, measured by ammonium chloride treatment at the end of the experiments. Conversion of GCaMP6f fluorescence to a Ca²⁺ concentration was accomplished by inverting the Hill equation of fluorescence vs. [Ca²⁺] as previously described (35). In brief, to linearize the GCaMP6f signal, the fluorescence signal was converted to the signal relative to that obtained with MgGreen using the equation. These linearized values were normalized to the average of the first stimulation to estimate the paired-pulse Ca²⁺ responses in excitatory neurons.

Quantification and Statistical Analysis. Statistical analyses were performed in Excel and Origin. We used paired two sample for means t test for paired results. Normally distributed data were processed with the Student's t test for two independent distributions with a one-way ANOVA followed by Tukey's post hoc comparison for comparing more than two groups to examine statistical significance. We specify the use of these tests and exact sample sizes in the figure legends for clarity.

Data Availability. All relevant data, associated protocols, and materials are provided in *Materials and Methods* and *SI Appendix*. Plasmids have been deposited in Addgene for distribution to all interested researchers under accession number 78223.

ACKNOWLEDGMENTS. We thank Andrew Coleman, Kelly Forest, Michelle Gleason, and Amelia Ralowicz for critical reading of the manuscript. This work was supported by the Esther A. and Joseph Klingenstein Fund (S.A.A., M.B.H.); NSF Grant IOS 1750199 (to I.H.C., M.B.H.); US Department of Education Graduate Assistance in Areas of National Need Grant P200A150059 (to S.A.A.); NIH Grant F31NS110192-01A1 (to L.C.P.); P20 NIGMS Grant GM113132 (to M.B.H.); and Grants R00-NS099469 and P20-GM113132 (to R.A.H.).

- S. Y. Kawaguchi, T. Sakaba, Control of inhibitory synaptic outputs by low excitability of axon terminals revealed by direct recording. *Neuron* 85, 1273–1288 (2015).
- J. Qian, P. Saggau, Activity-dependent modulation of K+ currents at presynaptic terminals of mammalian central synapses. J. Physiol. 519, 427–437 (1999).
- B. Chanda et al., A hybrid approach to measuring electrical activity in genetically specified neurons. Nat. Neurosci. 8, 1619–1626 (2005).
- M. B. Hoppa, G. Gouzer, M. Armbruster, T. A. Ryan, Control and plasticity of the presynaptic action potential waveform at small CNS nerve terminals. *Neuron* 84, 778–789 (2014).
- A. Bialowas et al., Analog modulation of spike-evoked transmission in CA3 circuits is determined by axonal Kv1.1 channels in a time-dependent manner. Eur. J. Neurosci. 41, 293–304 (2015).
- J. Balaji, T. A. Ryan, Single-vesicle imaging reveals that synaptic vesicle exocytosis and endocytosis are coupled by a single stochastic mode. *Proc. Natl. Acad. Sci. U.S.A.* 104, 20576–20581 (2007).
- D. R. Hochbaum et al., All-optical electrophysiology in mammalian neurons using engineered microbial rhodopsins. Nat. Methods 11, 825–833 (2014).
- I. H. Cho, L. C. Panzera, M. Chin, M. B. Hoppa, Sodium channel β2 subunits prevent action potential propagation failures at axonal branch points. *J. Neurosci.* 37, 9519–9533 (2017).
- L. Z. Fan et al., All-optical electrophysiology reveals the role of lateral inhibition in sensory processing in cortical layer 1. Cell 180, 521–535.e18 (2020).
- F. A. Dobie, A. M. Craig, Inhibitory synapse dynamics: Coordinated presynaptic and postsynaptic mobility and the major contribution of recycled vesicles to new synapse formation. J. Neurosci. 31, 10481–10493 (2011).
- S. Boudkkazi, L. Fronzaroli-Molinieres, D. Debanne, Presynaptic action potential waveform determines cortical synaptic latency. J. Physiol. 589, 1117–1131 (2011).
- J. S. Dittman, A. C. Kreitzer, W. G. Regehr, Interplay between facilitation, depression, and residual calcium at three presynaptic terminals. J. Neurosci. 20, 1374–1385 (2000).
- L. E. Dobrunz, E. P. Huang, C. F. Stevens, Very short-term plasticity in hippocampal synapses. Proc. Natl. Acad. Sci. U.S.A. 94, 14843–14847 (1997).
- J. T. Lock, I. Parker, I. F. Smith, A comparison of fluorescent Ca²⁺ indicators for imaging local Ca²⁺ signals in cultured cells. Cell Calcium 58, 638–648 (2015).
- B. L. Sabatini, W. G. Regehr, Optical measurement of presynaptic calcium currents. Biophys. J. 74, 1549–1563 (1998).
- E. M. Adler, G. J. Augustine, S. N. Duffy, M. P. Charlton, Alien intracellular calcium chelators attenuate neurotransmitter release at the squid giant synapse. *J. Neurosci.* 11. 1496–1507 (1991).
- M. B. Hoppa, B. Lana, W. Margas, A. C. Dolphin, T. A. Ryan, α2δ expression sets presynaptic calcium channel abundance and release probability. *Nature* 486, 122–125 (2012)
- T. Hoshi, W. N. Zagotta, R. W. Aldrich, Biophysical and molecular mechanisms of Shaker potassium channel inactivation. Science 250, 533–538 (1990).

- W. N. Zagotta, T. Hoshi, R. W. Aldrich, Restoration of inactivation in mutants of Shaker potassium channels by a peptide derived from ShB. Science 250, 568–571 (1990).
- J. Rettig et al., Inactivation properties of voltage-gated K+ channels altered by presence of beta-subunit. Nature 369, 289–294 (1994).
- O. Pongs, J. R. Schwarz, Ancillary subunits associated with voltage-dependent K+ channels. *Physiol. Rev.* 90, 755–796 (2010).
- G. Grosse et al., Expression of Kv1 potassium channels in mouse hippocampal primary cultures: Development and activity-dependent regulation. J. Neurosci. 20, 1869–1882 (2000).
- N. Helassa et al., Ultrafast glutamate sensors resolve high-frequency release at Schaffer collateral synapses. Proc. Natl. Acad. Sci. U.S.A. 115, 5594–5599 (2018).
- S. L. Jackman, J. Turecek, J. E. Belinsky, W. G. Regehr, The calcium sensor synaptotagmin 7 is required for synaptic facilitation. *Nature* 529, 88–91 (2016).
- K. P. Giese et al., Reduced K+ channel inactivation, spike broadening, and afterhyperpolarization in Kvbeta1.1-deficient mice with impaired learning. *Learn. Mem.* 5, 257–273 (1998).
- R. S. Zucker, W. G. Regehr, Short-term synaptic plasticity. Annu. Rev. Physiol. 64, 355–405 (2002).
- A. Bhalla, W. C. Tucker, E. R. Chapman, Synaptotagmin isoforms couple distinct ranges of Ca2+, Ba2+, and Sr2+ concentration to SNARE-mediated membrane fusion. *Mol. Biol. Cell* 16, 4755–4764 (2005).
- C. Chen, R. Satterfield, S. M. Young Jr, P. Jonas, Triple function of synaptotagmin 7 ensures efficiency of high-frequency transmission at central GABAergic synapses. *Cell Rep.* 21, 2082–2089 (2017).
- 47. F. Luo, T. C. Sudhof, Synaptotagmin-7-mediated asynchronous release boosts high-fidelity synchronous transmission at a central synapse. *Neuron* **94**, 826–839.e3 (2017).
- D. D. MacDougall et al., The high-affinity calcium sensor synaptotagmin-7 serves multiple roles in regulated exocytosis. J. Gen. Physiol. 150, 783–807 (2018).

- J. Turecek, S. L. Jackman, W. G. Regehr, Synaptotagmin 7 confers frequency invariance onto specialized depressing synapses. *Nature* 551, 503–506 (2017).
- V. Tran, C. Stricker, Diffusion of Ca²⁺ from small boutons en passant into the axon shapes AP-evoked Ca²⁺ transients. *Biophys. J.* 115, 1344–1356 (2018).
- 51. P. Ariel, T. A. Ryan, Optical mapping of release properties in synapses. Front. Neural Circuits 4, 18 (2010).
- Y. P. Tan, I. Llano, Modulation by K+ channels of action potential-evoked intracellular Ca2+ concentration rises in rat cerebellar basket cell axons. J. Physiol. 520, 65–78 (1999).
- R. Begum, Y. Bakiri, K. E. Volynski, D. M. Kullmann, Action potential broadening in a presynaptic channelopathy. *Nat. Commun.* 7, 12102 (2016).
- A. Lee, T. Scheuer, W. A. Catterall, Ca2+/calmodulin-dependent facilitation and inactivation of P/Q-type Ca2+ channels. J. Neurosci. 20, 6830–6838 (2000).
- C. Weyrer et al., The role of CaV2.1 channel facilitation in synaptic facilitation. Cell Rep. 26. 2289–2297.e3 (2019).
- Y. M. Yang et al., Enhancing the fidelity of neurotransmission by activity-dependent facilitation of presynaptic potassium currents. Nat. Commun. 5, 4564 (2014).
- S. W. Chouinard, G. F. Wilson, A. K. Schlimgen, B. Ganetzky, A potassium channel beta subunit related to the aldo-keto reductase superfamily is encoded by the Drosophila hyperkinetic locus. *Proc. Natl. Acad. Sci. U.S.A.* 92, 6763–6767 (1995).
- U. Vivekananda et al., Kv1.1 channelopathy abolishes presynaptic spike width modulation by subthreshold somatic depolarization. Proc. Natl. Acad. Sci. U.S.A. 114, 2395–2400 (2017).
- S. M. Voglmaier et al., Distinct endocytic pathways control the rate and extent of synaptic vesicle protein recycling. Neuron 51, 71–84 (2006).
- S. A. Alpizar, A. L. Baker, A. T. Gulledge, M. B. Hoppa, Loss of neurofascin-186 disrupts alignment of AnkyrinG relative to its binding partners in the axon initial segment. Front. Cell. Neurosci. 13, 1 (2019).